The Journal of Immunology



# Chaperone-Mediated Autophagy Suppresses Apoptosis via Regulation of the Unfolded Protein Response during Chronic Obstructive Pulmonary Disease Pathogenesis

Yusuke Hosaka, Jun Araya, Yu Fujita, Tsukasa Kadota, Kazuya Tsubouchi, Masahiro Yoshida, Shunsuke Minagawa, Hiromichi Hara, Hironori Kawamoto, Naoaki Watanabe, Akihiko Ito, Akihiro Ichikawa, Nayuta Saito, Keitaro Okuda, Junko Watanabe, Daisuke Takekoshi, Hirofumi Utsumi, Mitsuo Hashimoto, Hiroshi Wakui, Saburo Ito, Takanori Numata, Shohei Mori, Hideki Matsudaira, Jun Hirano, Takashi Ohtsuka, Katsutoshi Nakayama and Kazuyoshi Kuwano

*J Immunol* published online 22 July 2020
http://www.jimmunol.org/content/early/2020/07/21/jimmunol.2000132



*The Journal of Immunology* is published twice each month by The American Association of Immunologists, Inc., 1451 Rockville Pike, Suite 650, Rockville, MD 20852

Print ISSN: 0022-1767 Online ISSN: 1550-6606.

Published July 22, 2020, doi:10.4049/jimmunol.2000132



# Chaperone-Mediated Autophagy Suppresses Apoptosis via Regulation of the Unfolded Protein Response during Chronic Obstructive Pulmonary Disease Pathogenesis

**Yusuke Hosaka,*,[1] Jun Araya,*,[1] Yu Fujita,* Tsukasa Kadota,* Kazuya Tsubouchi,* Masahiro Yoshida,* Shunsuke Minagawa,* Hiromichi Hara,* Hironori Kawamoto,* Naoaki Watanabe,* Akihiko Ito,* Akihiro Ichikawa,* Nayuta Saito,* Keitaro Okuda,* Junko Watanabe,* Daisuke Takekoshi,* Hirofumi Utsumi,* Mitsuo Hashimoto,* Hiroshi Wakui,* Saburo Ito,* Takanori Numata,* Shohei Mori,† Hideki Matsudaira,† Jun Hirano,† Takashi Ohtsuka,† Katsutoshi Nakayama,‡ and Kazuyoshi Kuwano***

**Cigarette smoke (CS) induces accumulation of misfolded proteins with concomitantly enhanced unfolded protein response (UPR). Increased apoptosis linked to UPR has been demonstrated in chronic obstructive pulmonary disease (COPD) pathogenesis. Chaperone-mediated autophagy (CMA) is a type of selective autophagy for lysosomal degradation of proteins with the KFERQ peptide motif. CMA has been implicated in not only maintaining nutritional homeostasis but also adapting the cell to stressed conditions. Although recent papers have shown functional cross-talk between UPR and CMA, mechanistic implications for CMA in COPD pathogenesis, especially in association with CS-evoked UPR, remain obscure. In this study, we sought to examine the role of CMA in regulating CS-induced apoptosis linked to UPR during COPD pathogenesis using human bronchial epithelial cells (HBEC) and lung tissues. CS extract (CSE) induced LAMP2A expression and CMA activation through a Nrf2-dependent manner in HBEC. LAMP2A knockdown and the subsequent CMA inhibition enhanced UPR, including CHOP expression, and was accompanied by increased apoptosis during CSE exposure, which was reversed by LAMP2A overexpression. Immunohistochemistry showed that Nrf2 and LAMP2A levels were reduced in small airway epithelial cells in COPD compared with non-COPD lungs. Both Nrf2 and LAMP2A levels were significantly reduced in HBEC isolated from COPD, whereas LAMP2A levels in HBEC were positively correlated with pulmonary function tests. These findings suggest the existence of functional cross-talk between CMA and UPR during CSE exposure and also that impaired CMA may be causally associated with COPD pathogenesis through enhanced UPR-mediated apoptosis in epithelial cells.** ***The Journal of Immunology*****, 2020, 205: 000–000.**

Chronic obstructive pulmonary disease (COPD) caused by cigarette smoke (CS) exposure is a leading cause of death worldwide. COPD is characterized by airflow limitation, which is progressive even after smoking cessation (1). Each puff of CS contains ~$10^{17}$ oxidant molecules, and accumulating evidence indicates that oxidative stress has an essential role in COPD development (2). CS induces oxidative modifications to a wide array of lung macromolecules including proteins, resulting in the accumulation of damaged and misfolded proteins with concomitantly enhanced unfolded protein response (UPR) (3, 4). Although UPR is generally a cytoprotective mechanism, reversing endoplasmic reticulum (ER) stress through protein chaperoning and slowing the flow of newly synthesized polypeptides into the ER, UPR also plays a role in apoptosis induction during excessive ER stress (5). Increased apoptosis in epithelial cells associated with UPR has been demonstrated in COPD lungs, and apoptosis has been widely implicated in COPD progression (5–10). Accordingly, UPR linked to CS-induced oxidative modifications and subsequent apoptosis may have a regulatory role in COPD pathogenesis.

During UPR, dsRNA-activated protein kinase–like ER kinase (PERK) promotes expression of NFE2L2/Nrf2 by inactivating its

*Division of Respiratory Diseases, Department of Internal Medicine, Jikei University School of Medicine, Tokyo 104-8461, Japan; †Division of Chest Diseases, Department of Surgery, Jikei University School of Medicine, Tokyo 104-8461, Japan; and ‡Department of Respiratory Medicine, Akita University Graduate School of Medicine, Akita 010-8543, Japan

[1]Y.H. and J.A. contributed equally to this work.

ORCIDs: 0000-0002-8916-7303 (Y.F.); 0000-0003-0145-8745 (K.T.); 0000-0003-1732-4856 (S. Minagawa); 0000-0001-5783-5998 (A. Ito); 0000-0002-9314-4745 (N.S.); 0000-0003-2784-2331 (T.N.); 0000-0002-8817-275X (H.M.); 0000-0002-8039-9159 (T.O.); 0000-0002-0141-7081 (K.N.); 0000-0003-0551-7386 (K.K.).

Received for publication February 5, 2020. Accepted for publication June 29, 2020.

This work was supported by Japan Society for the Promotion of Science KAKENHI Grants JP18K08158 (to J.A.), JP19K17649 (to Y.F.), JP17K09673 (to S. Minagawa), JP19K08632 (to H.H.), JP17K09672 (to T.N.), JP19K08612 (to H.U.), and JP17K09674 (to M.H.).

Address correspondence and reprint requests to Dr. Jun Araya, Jikei University School of Medicine, 3-25-8 Nishi-shimbashi, Minato-ku, Tokyo 105-8461, Japan. E-mail address: araya@jikei.ac.jp

The online version of this article contains supplemental material.

Abbreviations used in this article: CMA, chaperone-mediated autophagy; COPD, chronic obstructive pulmonary disease; CS, cigarette smoke; CSE, CS extract; ER, endoplasmic reticulum; %FEV1.0, percentage of predicted forced expiratory volume in 1 s; HBEC, human bronchial epithelial cell; LAMP2A, lysosomal-associated membrane protein type 2A; LDH, lactate dehydrogenase; miRNA, microRNA; NAC, *N*-acetyl cysteine; PERK, protein kinase–like ER kinase; PI, propidium iodide; SAEC, small airway epithelial cell; SI, smoking index; siRNA, small interfering RNA; UPR, unfolded protein response.

cytoplasmic inhibitor, Kelch-like ECH-associated protein 1 (5, 11). Nrf2 is a master transcription factor, orchestrating the antioxidant defense system via expression of a variety of antioxidant enzymes, and has also been implicated in redox homeostasis and cell survival during oxidative stress (12). Nrf2 is abundant in the lung and is involved in the pathogenesis of lung disorders in which the balance between oxidative stress and antioxidants is lacking (12). Decreased Nrf2 expression in macrophages and epithelial cells has been implicated in COPD pathogenesis (2, 13). A causal link between Nrf2 reduction and COPD pathogenesis was further demonstrated by exaggerated emphysematous changes accompanied by increased lung inflammation and lung epithelial cell apoptosis in CS-exposed Nrf2-deficient mice (14). Thus, Nrf2 expression levels can be a critical determinant of oxidative damage in those COPD lungs with increased UPR. Intriguingly, a recent paper showed that Nrf2 also activates chaperone-mediated autophagy (CMA) via upregulating the lysosomal-associated membrane protein type 2A (LAMP2A) (15).

CMA is a type of autophagy, an essential homeostatic process for lysosomal degradation of cellular components. Among the three major autophagic pathways, CMA is responsible for selective degradation of proteins with the KFERQ peptide motif or a related sequence (16). During CMA, heat shock cognate 71 kDa protein recognizes the KFERQ peptide motif, whereas LAMP2A is involved in substrate binding and internalization to lysosome, respectively. Lysosomal expression level of LAMP2A is considered to be the rate-limiting factor for the CMA pathway (16). Approximately 40% of proteins in the mammalian proteome contain a canonical KFERQ-like motif, and there is a wide array of physiological roles for CMA-mediated proteostasis in metabolic pathways, transcriptional regulation, immune response, and cell cycle (16). Impairment of CMA has been implicated in aging-associated pathology, including neurodegenerative disorders through the accumulation of damaged proteins. COPD is a representative aging-related pulmonary disorder, and aberrant macroautophagic activity has been demonstrated in its pathogenesis (17–20). There is functional compensatory cross-talk between macroautophagy and CMA (21). Furthermore, a recent paper showed that UPR actives CMA via p38-mediated phosphorylation of LAMP2A, indicating that CMA-regulated proteostasis may have an essential role in COPD pathogenesis in the setting of altered UPR and macroautophagy (22). Although the potential participation of CMA in CS extract (CSE)–induced epithelial cell apoptosis has been reported (23), a mechanistic implication for CMA in COPD pathogenesis, especially in terms of CS-mediated UPR, remains obscure.

In the current study, we examined the regulatory role of Nrf2-mediated LAMP2A expression in CMA activation by CS and the involvement of CMA in modulating CS-induced UPR and apoptosis during COPD pathogenesis.

## Materials and Methods

### *Cell culture, Abs, and reagents*

Normal and COPD airways were collected from first through fourth order bronchi from pneumonectomy and lobectomy specimens from resections performed for primary lung cancer. Informed consent was obtained from all surgical participants as part of an approved ongoing research protocol by the ethical committee of Jikei University School of Medicine [23-153(5443)]. Human bronchial epithelial cells (HBECs) were isolated with protease treatment, and freshly isolated HBECs were plated onto rat tail collagen type I–coated (10 μg/ml) dishes and incubated overnight, and then the medium was changed to bronchial epithelial growth medium (Lonza, Tokyo, Japan) (24). Cultures were characterized immunohistochemically using anticytokeratin Abs (Lu-5; BioCare Medical, Concord, CA) and antivimentin (Sigma-Aldrich, Tokyo, Japan). HBEC showed >95% positive staining with anticytokeratin and <5% positive staining with antivimentin Ab (data not shown). HBEC were serially passed and used for experiments until passage 3. Most experiments were performed with HBEC from non-COPD patients. Small airway epithelial cells (SAEC) and SAEC growth medium were purchased (Lonza). The bronchial epithelial cell line BEAS-2B was cultured in RPMI 1640 (no. 11875-093; Gibco Life Technologies) with 10% FCS (no. 26140-079; Life Technologies) and penicillin–streptomycin (no. 15070-063; Life Technologies). Abs used were rabbit anti-LAMP2A (no. ab125068; abcam), rabbit anti-Nrf2 (no. ab62352; abcam), rabbit anti-LAMP1 (no. 9091; Cell Signaling Technology), mouse anti-CHOP (no. ab11419; abcam), rabbit anti–caspase-3 (no. 14220; Cell Signaling Technology), rabbit anti-Bip (no. 3177; Cell Signaling Technology), rabbit anti-eIF2α (no. 9722; Cell Signaling Technology), rabbit anti–phospho-eIF2α (no. 3398; Cell Signaling Technology), rabbit anti-ATF4 (no. 11815; Cell Signaling Technology), rabbit anti-GAPDH (no. 5174; Cell Signaling Technology), mouse anti-ACTB (no. A5316; Sigma-Aldrich), DAPI (no. R37606; Invitrogen), *N*-acetyl-L-cysteine (no. 017–5131; FUJIFILM Wako Pure Chemical), caspase inhibitor Z-VAD-FMK(no. G7231; Promega), and collagen type I solution from rat tail (no. C3867; Sigma-Aldrich) were purchased.

### *Plasmids, small interfering RNA, and transfection*

LAMP2A expression vector (no. RC221216; OriGene) was purchased from OriGene. Small interfering RNA (siRNA) targeting *Nrf2* (no. s9492, no. s9493; Applied Biosystems, Life Technologies), *CHOP* (no. n353816, no. n353819; Applied Biosystems, Life Technologies), and negative control siRNAs (no. AM4635, no. AM4641; Applied Biosystems, Life Technologies) were purchased from Life Technologies. *LAMP2A* siRNA was designed by using BLOCK-iT RNAi Designer (https://rnaidesigner.thermofisher.com). The sequences of the regions targeted by the siRNA in the exon of the *LAMP2A* gene were 5′-GCAGTGCAGATGACGACAA-3′ and 5′-GCACCATCATGCTGGATAT-3′, corresponding to bases 1230–1248 and 1330–1348, respectively. Specific knockdowns of Nrf2, LAMP2A, and CHOP were validated using two different siRNA, respectively. Transfections of HBEC and BEAS-2B cells were performed using the Neon Transfection System (no. MPK5000; Invitrogen, Life Technologies), using matched optimized transfection kits (no. MPK10096; Invitrogen, Life Technologies).

### *Preparation of CSE*

CSE was prepared as previously described (24). Forty milliliters of CS were drawn into the syringe and slowly bubbled into sterile serum-free cell culture media in 15-ml BD Falcon tubes. One cigarette was used for the preparation of 10 ml of solution. CSE solution was filtered (no. SLGS033SS, 0.22 μm; MilliporeSigma) to remove insoluble particles and was designated as a 100% CSE solution.

### *RNA isolation and PCR*

RNA isolation, reverse transcription, and real-time PCR were performed using the SYBR Green method as previously described (24). The primers used were LAMP2A sense primer, 5′-GCACAGTGAGCACAAATGAGT-3′; LAMP2A antisense primer, 5′-CAGTGGTGTGTATGGTGGGT-3′; Nrf2 sense primer, 5′-TCAGCGACGGAAAGAGTATGA-3′; Nrf2 antisense primer, 5′-CCACTGGTTTCTGACTGGATGT-3′; CHOP sense primer, 5′-GAACGGCTCAAGCAGGAAATC-3′; CHOP antisense primer, 5′-TTCACCATTCGGTCAATCAGAG-3′; ACTB sense primer, 5′-CATGTACGTTGCTATCCAGGC-3′; and ACTB antisense primer, 5′-CTCCTTAATGTCACGCACGAT-3′. These primer sets yielded PCR products of 75, 174, 80, and 250 bp for LAMP2A, Nrf2, CHOP, and ACTB respectively. PCRs of LAMP2A, Nrf2, CHOP, and ACTB were validated using two different primers. Primer sequences were from PrimerBank (http://pga.mgh.harvard.edu/primerbank).

### *Immunohistochemistry and immunofluorescence staining*

Immunohistochemical staining was performed as previously described with a minor modification on the paraffin-embedded lung tissues (24). LAMP2A, Nrf2, LAMP1, and Bip immunostaining were assessed by measuring areas of total and positively staining cells in small airways at a magnification of ×400 using ImageJ, an open source image processing program.

### *Western blotting*

HBEC and BEAS-2B grown on 6–12-well culture plates were lysed in RIPA buffer (no. 89900; Thermo Fisher Scientific) with protease inhibitor mixture (no. 11697498001; Roche Diagnostics) and 1 mM sodium orthovanadate or lysed with Laemmli sample buffer. Western blotting was

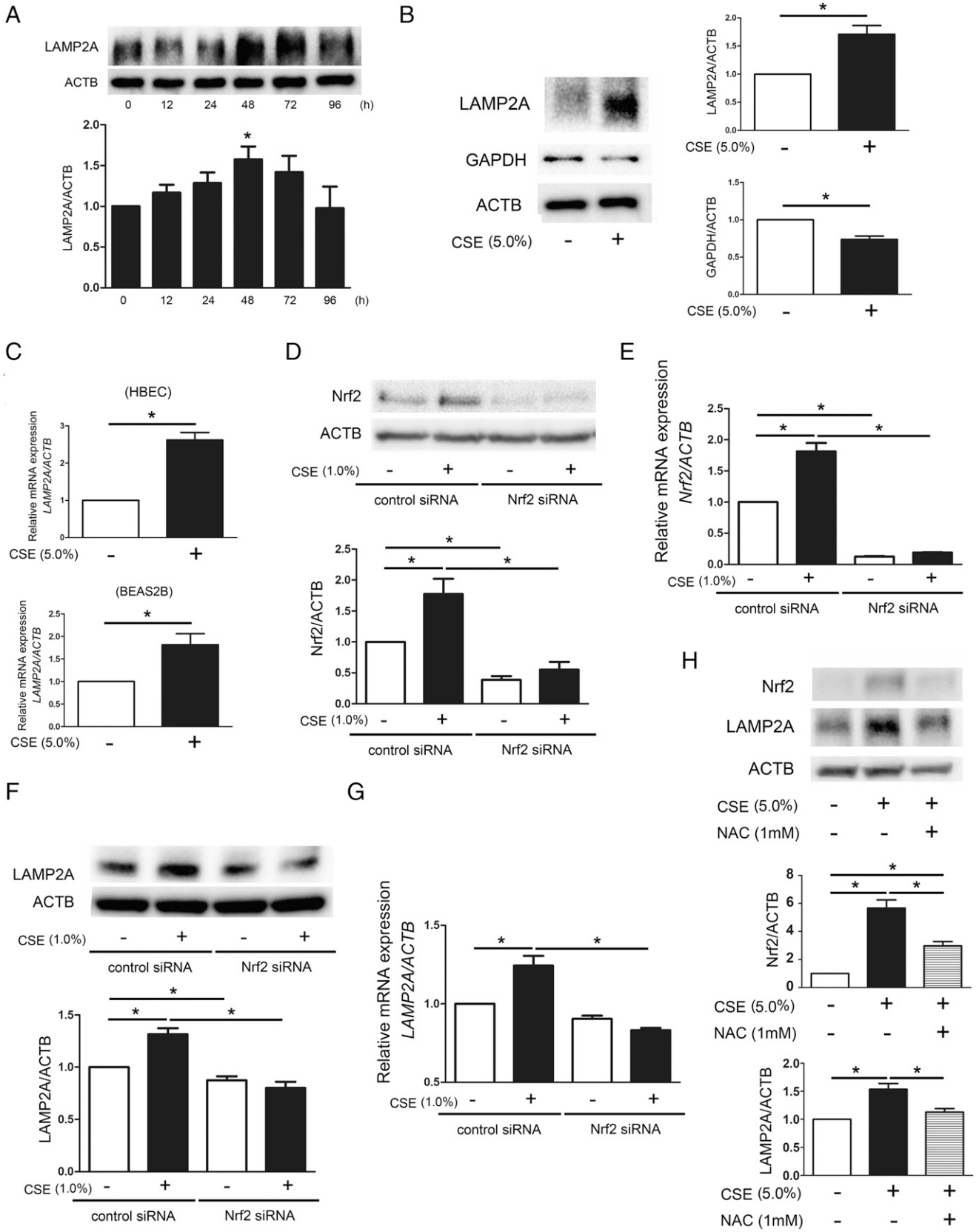


**FIGURE 1.** Nrf2 is involved in the mechanisms for CSE-induced LAMP2A expression. (**A**) Western blotting (WB) using anti-LAMP2A and anti-ACTB of HBEC lysates are treated with CSE (5%) for the indicated time. The lower panel shows the average (±SEM) of relative expression, taken from densitometric analysis of WB ($n = 3$). (**B**) WB using anti-LAMP2A and anti-ACTB of BEAS-2B cell lysates treated with CSE (5%) for 48 h. The right panel shows the average (±SEM) of relative expression, taken from densitometric analysis of WB ($n = 3$). (**C**) Real-time PCR was performed using primers to LAMP2A or ACTB as a control. LAMP2A mRNA expression was normalized to ACTB. RNA samples were collected after treatment with CSE (1%) for 24 h. Upper panel is HBEC, and lower panel is BEAS-2B cell. Shown is the fold increase (±SEM) relative to control-treated cells ($n = 3$). (**D**) WB using anti-Nrf2 and anti-ACTB. BEAS-2B cells were transfected with control or Nrf2 siRNA, and CSE treatment was started 48 h post-siRNA transfection. Cell lysates were collected *(Figure legend continues)*

performed as previously described (25). For each experiment, equal amounts of total protein were resolved by 4–20% SDS-PAGE. After SDS-PAGE, proteins were transferred to polyvinylidene difluoride membrane (no. ISEQ00010; MilliporeSigma), and incubation with specific primary Ab was performed for 2 h at 37˚C or 24 h at 4˚C. After washing several times with PBS with Tween 20, the membrane was incubated with anti-rabbit IgG, HRP-linked secondary Ab (no. 7074; Cell Signaling Technology) or anti-mouse IgG, HRP-linked secondary Ab (no. 7076; Cell Signaling Technology) followed by chemiluminescence detection (no. 34080; Thermo Fisher Scientific and no. 1705061; Bio-Rad Laboratories) with the ChemiDoc Touch Imaging System (Bio-Rad Laboratories).

### *MTT assay*

The MTT assay was performed according to the manufacturer's instructions (no. 11465007001; Roche Diagnostics).

### *Lactate dehydrogenase assay*

Cell death was assessed by cytotoxicity analyzed by measuring the release of lactate dehydrogenase (LDH) into media according to the manufacturer's protocol (no. 4744926; Roche Diagnostics).

### *TUNEL assay*

TUNEL assay was performed using a DeadEnd Fluorometric TUNEL System (G3250; Promega), according to the manufacturer's instructions. The TUNEL-positive cells in the lung were detected using fluorescence microscopy (Nikon, Tokyo, Japan). The average number of dead cells was assessed by manual counting of $TUNEL^+$ cells in each high- power field (×200).

### *Flow cytometry by annexin V–FITC conjugated with propidium iodide staining*

Apoptosis was evaluated by flow cytometry, using annexin V–FITC and propidium iodide (PI) double staining following the manufacturer's instructions for the MEBCYTO apoptosis kit (MBL, Nagoya, Japan) (23). Cells in each treated group were washed twice with cold PBS and then resuspended in binding buffer. A total of $1 \times 10^6$ cells/ml were transferred in a 5-ml tube containing 10 μl of annexin V–FITC and 5 μl of PI and were incubated for 15 min at room temperature in the dark. After adding 400 μl of binding buffer, the samples were analyzed by flow cytometry (MACSQuant, Miltenyi Biotec, Bergisch Gladbach, Germany) within 1 h. Annexin V–positive cells were considered apoptotic cells. Data analysis was performed with FlowJo software.

### *Statistics*

Data are shown as the average (±SEM) taken from at least three independent experiments. Student *t* test was used for comparison of two datasets, ANOVA was used for multiple comparisons, and Bonferroni post hoc tests were used to test for statistical significance. Significance was defined as $p < 0.05$. The statistical software used was Prism v.7 (GraphPad Software, San Diego, CA).

## Results

### *CSE-induced LAMP2A expression is dependent on Nrf2*

Initially, we examined changes in LAMP2A expression in response to CSE exposure. CSE (5.0%) treatment significantly increased protein levels of LAMP2A in HBEC, which peaked at 48 h after CSE exposure (Fig. 1A). CSE also significantly induced LAMP2A expression at 48 h in BEAS-2B cells (Fig. 1B). Along with increased LAMP2A protein levels, GAPDH, a representative selective target protein for CMA degradation, was clearly reduced, which may reflect increased CMA activity (Fig. 1B). Increased LAMP2A mRNA caused by CSE exposure was confirmed by RT-PCR in both HBEC and BEAS-2B cells (Fig. 1C).

To elucidate the involvement of Nrf2 in regulating LAMP2A expression, siRNA-mediated Nrf2 knockdown was performed in BEAS-2B cells. Because Nrf2 knockdown was highly toxic during CSE exposure, we selected 1.0% CSE for Nrf2 knockdown experiments. CSE significantly increased Nrf2 expression at both protein and mRNA level, which were efficiently suppressed by siRNA transfection (Fig. 1D, 1E). In line with recent reports, Nrf2 knockdown significantly inhibited CSE-induced LAMP2A protein expression (Fig. 1F), suggesting Nrf2 is responsible for regulating LAMP2A expression during CSE exposure (15). Involvement of Nrf2 in LAMP2A mRNA expression during CSE exposure was confirmed by reduced LAMP2A mRNA levels during Nrf2 knockdown (Fig. 1G). In general, Nrf2 is activated in response to oxidative stress, and CS contains abundant oxidants; hence, participation of reactive oxygen species in CSE-induced Nrf2 expression was examined by treatment with the antioxidant *N*-acetyl cysteine (NAC). NAC significantly suppressed CSE induction of both Nrf2 and LAMP2A (Fig. 1H). Because Nrf2 has also been implicated in regulating macroautophagy-related genes (26), involvement of Nrf2 in macroautophagy was examined by CSE exposure. In comparison with LAMP2A, only a modest reduction of LC3 conversion was demonstrated in the setting of Nrf2 knockdown, suggesting that Nrf2 is mainly involved in CMA rather than macroautophagy during CSE exposure in HBEC (Supplemental Fig. 1A).

### *LAMP2A negatively regulates apoptosis in response to CSE exposure*

Nrf2-mediated LAMP2A expression suggests that CMA activation may have a protective role in CSE-induced oxidative stress, and CMA has been implicated in apoptosis inhibition during CSE exposure (23). LAMP2A knockdown experiments were performed to examine the role of CMA in apoptosis regulation in BEAS-2B cells. Efficient LAMP2A knockdown was confirmed by RT-PCR and Western blotting (data not shown). CSE suppressed viable cell counts and increased cell death as shown by MTT assay and LDH cytotoxic assay, which were significantly enhanced by LAMP2A knockdown (Fig. 2A, 2B). CSE-induced TUNEL-positive staining was also significantly increased by LAMP2A knockdown (Fig. 2C). CSE-induced apoptosis was evaluated by detecting expression levels of cleaved caspase-3 and increased percentage of annexin V–positive staining (Fig. 2D, 2E). CSE induced cleaved caspase-3 expression, which was further enhanced by LAMP2A knockdown (Fig. 2D). The increase in annexin V positively staining cells in the setting of LAMP2A knockdown was clearly suppressed by treatment with Z-VAD-FMK, a pan-caspase

after treatment with CSE (1%) for 48 h. The lower panel shows the average (±SEM) of relative expression, taken from densitometric analysis of WB ($n = 6$). (**E**) Real-time PCR was performed using primers to Nrf2 or ACTB as a control. BEAS-2B cells were transfected with control or Nrf2 siRNA, and CSE treatment was started 48 h post-siRNA transfection. RNA samples were collected after treatment with CSE (1%) for 24 h. Nrf2 mRNA expression was normalized to ACTB. Shown is the fold increase (±SEM) relative to control-treated cells ($n = 3$). (**F**) WB using anti-LAMP2A and anti-ACTB. BEAS-2B cells were transfected with control or Nrf2 siRNA, and CSE treatment was started 48 h post-siRNA transfection. Cell lysates were collected after treatment with CSE (1%) for 48 h. The lower panel shows the average (±SEM) of relative expression, taken from densitometric analysis of WB ($n = 3$). (**G**) Real-time PCR was performed using primers to LAMP2A or ACTB as a control. BEAS-2B cells were transfected with control or Nrf2 siRNA, and CSE treatment was started 48 h post-siRNA transfection. RNA samples were collected after treatment with CSE (1%) for 24 h. LAMP2A mRNA expression was normalized to ACTB. Shown is the fold increase (±SEM) relative to control-treated cells ($n = 3$). (**H**) WB using anti-Nrf2, anti-LAMP2A, and anti-ACTB of BEAS-2B cell lysates treated with CSE (5%) for 48 h in the absence or presence of NAC (1 mM). The lower panel shows the average (±SEM) of relative expressions, which are taken from densitometric analysis of WB ($n = 3$). *$p < 0.05$ by ANOVA and Bonferroni posttest (A, D, and E–H) or Student t test (B and C).

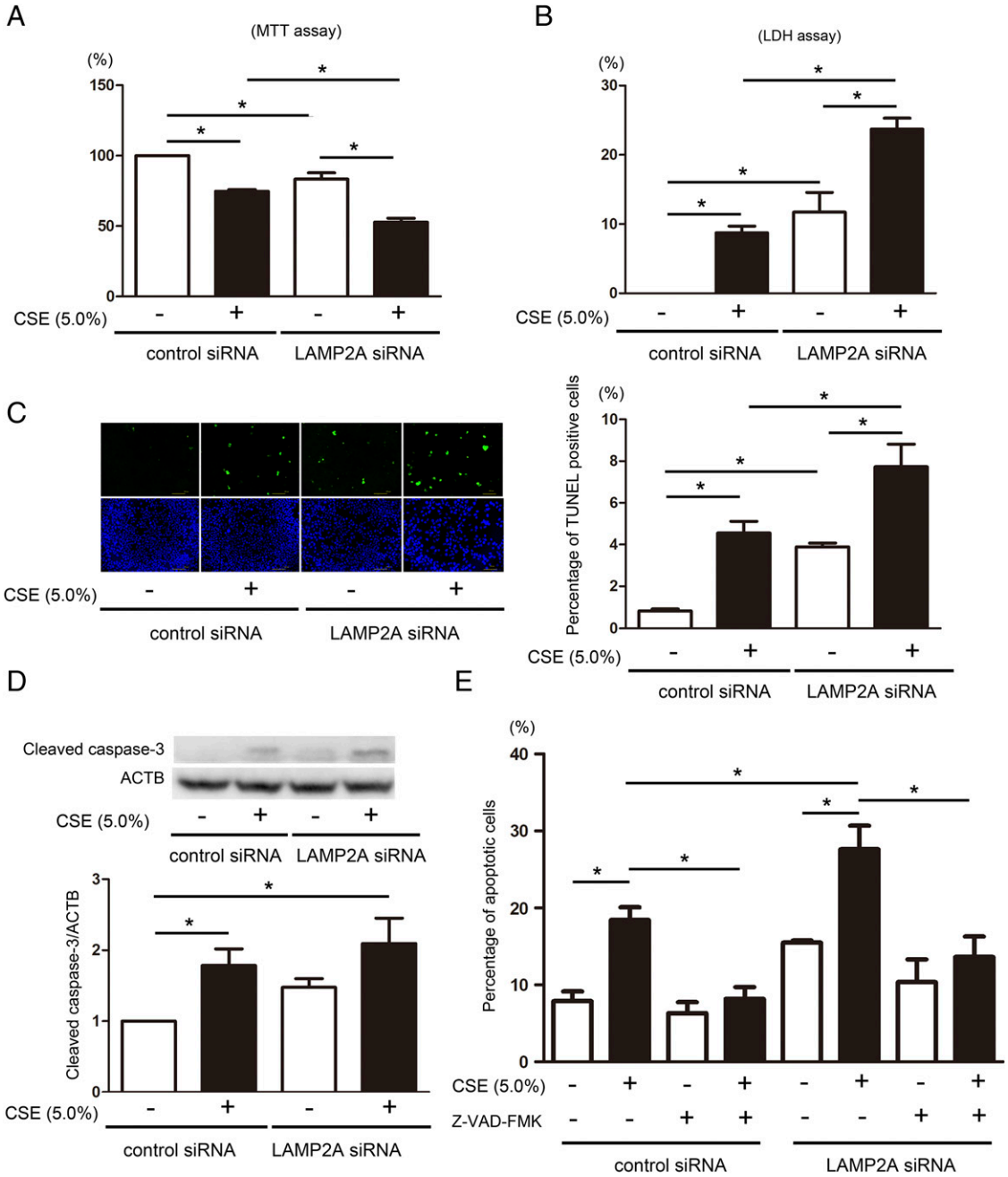


**FIGURE 2.** Inhibitory role of LAMP2A in CSE-induced apoptosis in BEAS-2B cells. (**A**) Viable cell counts were evaluated by MTT assay. BEAS-2B cells were transfected with control or LAMP2A siRNA, and CSE (5%) treatment was started 48 h post-siRNA transfection. Viable cell count was assessed after 24-h treatment. (**B**) Cell cytotoxicity analysis by the LDH assay. Cytotoxicity was calculated by measuring the amount of LDH in supernatant released from siRNA-transfected BEAS-2B cells after 24-h CSE (5%) treatment. (**C**) Photographs of fluorescence staining of the TUNEL assay of the control or LAMP2A siRNA-transfected BEAS-2B cells after 24-h treatment with CSE (5%). DAPI (blue) and TUNEL-positive cells (green) are shown. Scale bar, 100 μm. Right panel is the percentage of TUNEL-positive cells. (**D**) Western blotting (WB) using anti–caspase-3 and anti-ACTB. BEAS-2B cells were transfected with control or LAMP2A siRNA, and CSE treatment was started 48 h post-siRNA transfection. Cell lysates were collected after treatment with CSE (5%) for 24 h. The lower panel shows the average (±SEM) of relative expression, taken from densitometric analysis of WB ($n = 35$). (**E**) Apoptosis was detected by flow cytometric evaluation of FITC–annexin V and PI double staining. Percentage of apoptosis was calculated by adding early apoptotic cells (annexin $V^+/PI^-$) and late apoptotic/necrotic cells (annexin $V^+/PI^+$). CSE treatment was started 48 h post-siRNA transfection, and Z-VAD-FMK was pretreated for 1 h before CSE. *$p < 0.05$ by ANOVA and Bonferroni posttest.

inhibitor (Fig. 2E), indicating an antiapoptotic role for CMA-mediated LAMP2A expression during CSE exposure.

*LAMP2A reduction enhances CSE-induced UPR*

Increased UPR has been implicated in apoptosis in COPD pathogenesis (5–7). Among the three major pathways of UPR, we specifically focused on the apoptosis-linked PERK–CHOP pathway. CSE treatment significantly increased Bip, ATF4, and CHOP expression and induced eIF2a phosphorylation, which were further enhanced by LAMP2A knockdown in BEAS-2B cells (Fig. 3A–D). CHOP has an important role in conducting apoptosis in the PERK pathway during excessive ER stress. CSE-induced upregulation and LAMP2A knockdown-mediated enhancement of CHOP expression were confirmed at mRNA levels in both BEAS-2B cells and HBEC,

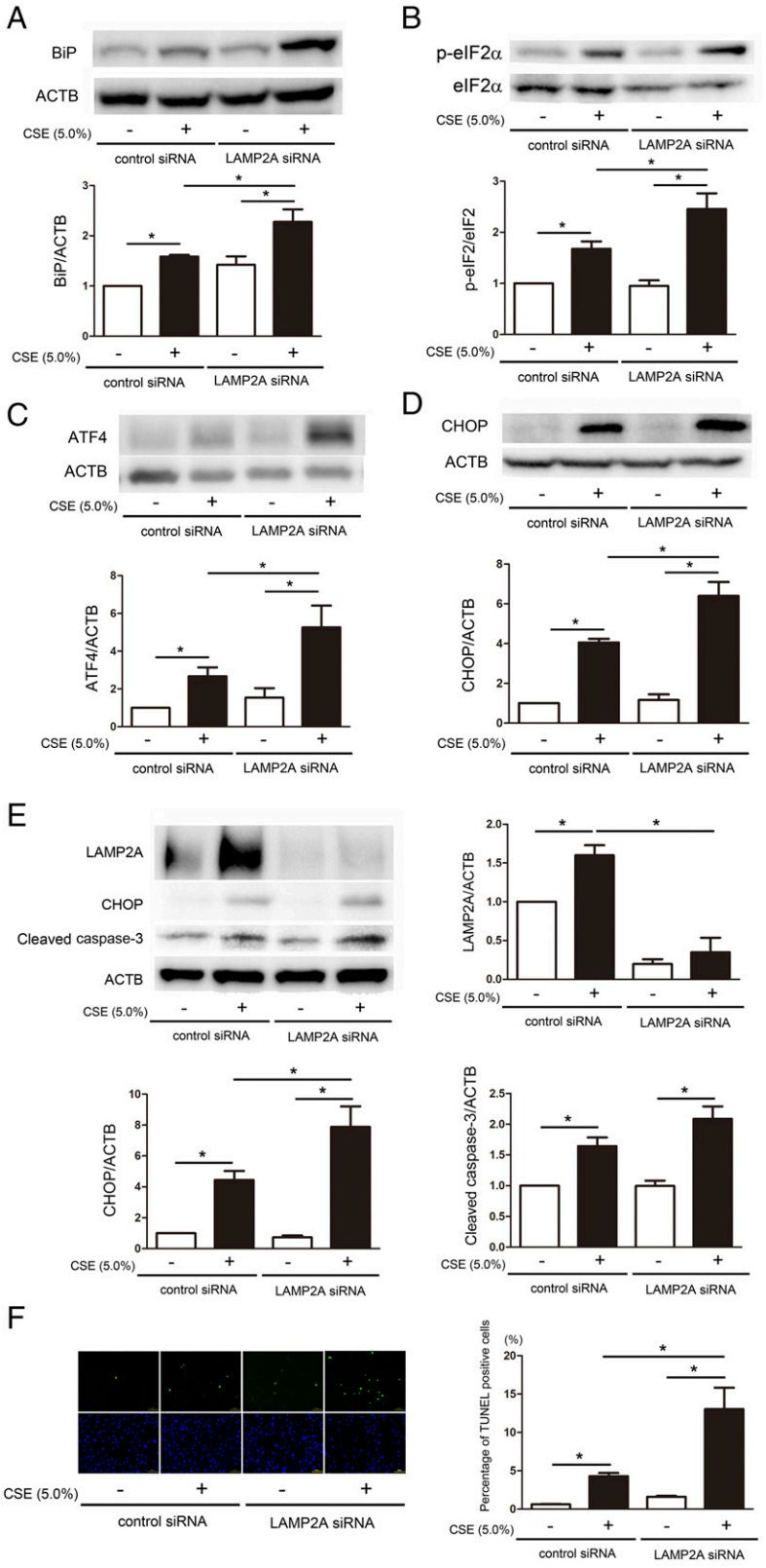


**FIGURE 3.** LAMP2A knockdown enhances CSE-induced UPR. (**A**) Western blotting (WB) using anti-Bip and anti-ACTB. BEAS-2B cells were transfected with control or LAMP2A siRNA, and CSE treatment was started 48 h post-siRNA transfection. Cell lysates were collected after treatment with CSE (5%) for 24 h. The lower panel shows the average (±SEM) of relative expression, taken from densitometric analysis of WB ($n$ = 5). (**B**) WB using anti–p-eIF2α and anti-eIF2α in BEAS-2B cells ($n$ = 7). (**C**) WB using anti-ATF4 and anti-ACTB in BEAS-2B cells ($n$ = 3). (**D**) WB using anti-CHOP and anti-ACTB in BEAS-2B cells ($n$ = 3). (**E**) WB using anti-LAMP2A, anti-CHOP, anticleaved caspase-3, and anti-ACTB. HBEC cells were transfected with control or LAMP2A siRNA, and CSE treatment was started 48 h post-siRNA transfection. Cell lysates were collected after treatment with CSE (5%) for 24 h. The panels show the average (±SEM) of relative expression, taken from densitometric analysis of WB ($n$ = 5). (**F**) Photographs of fluorescence staining of the TUNEL assay of the control or LAMP2A siRNA-transfected HBEC after 24-h treatment with CSE (5%). DAPI (blue) and TUNEL-positive cells (green) are shown. Scale bar, 100 μm. The right panel is the percentage of TUNEL-positive cells. *$p < 0.05$ by ANOVA and Bonferroni posttest.

respectively (Supplemental Fig. 1B, 1C). LAMP2A knockdown-mediated enhancement of CHOP protein levels and apoptosis by CSE exposure were also confirmed in HBEC (Fig. 3E, 3F). Because the small airways of <2 mm in diameter are mainly responsible for airway obstruction in COPD pathogenesis, we also evaluated the involvement of CMA using SAEC. Consistent with HBEC, CSE increased LAMP2A expression, which was suppressed by Nrf2 knockdown. LAMP2A knockdown clearly enhanced CSE-induced CHOP expression with concomitantly increased apoptosis (Supplemental Fig. 2).

Involvement of CHOP in CSE-induced apoptosis was further examined by means of siRNA-mediated CHOP knockdown. In BEAS-2B cells, CHOP knockdown significantly suppressed CSE-induced increases in TUNEL-positive cell count and caspase-3

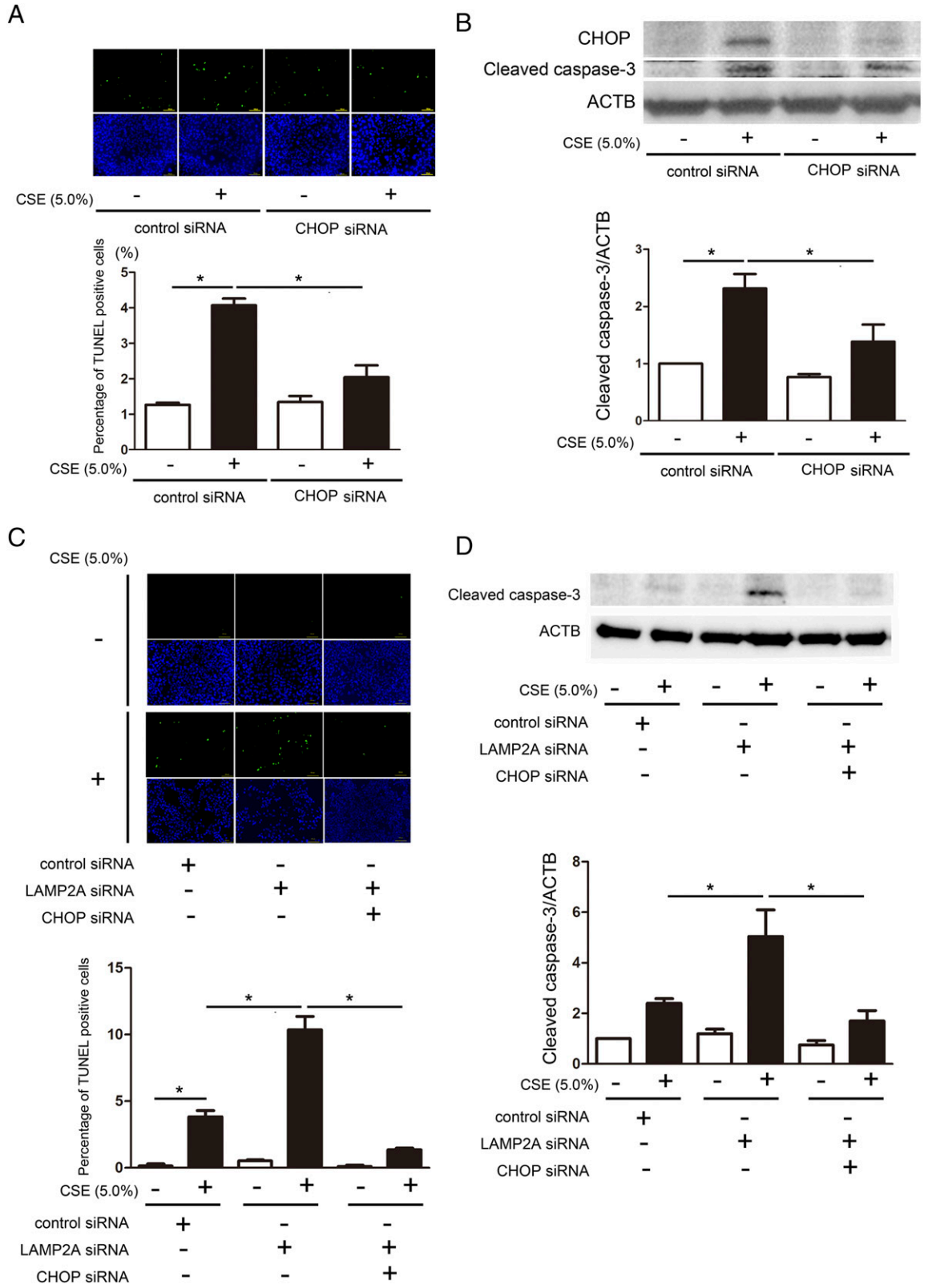


**FIGURE 4.** CHOP is involved in CSE-induced apoptosis. (**A**) Photographs of fluorescence staining of the TUNEL assay of the control or CHOP siRNA-transfected BEAS-2B cells after 24-h treatment with CSE (5%). CSE treatment was started 48 h post-siRNA transfection. DAPI (blue) and TUNEL-positive cells (green) are shown. Scale bar, 100 μm. The lower panel is the percentage of TUNEL-positive cells. (**B**) Western blotting (WB) using anti–caspase-3, anti-CHOP, and anti-ACTB. BEAS-2B cells were transfected with control or CHOP siRNA, and CSE treatment was started 48 h post-siRNA transfection. Cell lysates were collected after treatment with CSE (5%) for 24 h. The lower panel shows the average (±SEM) of relative expression, taken from densitometric analysis of WB ($n = 4$). (**C**) Photographs of fluorescence staining of the TUNEL assay of BEAS-2B cells. Control or LAMP2A siRNA was initially transfected, and control or CHOP siRNA was subsequently transfected after 24-h incubation. CSE (5%) treatment for 24 h was started 24 h post-siRNA transfection. DAPI (blue) and TUNEL-positive cells (green) are shown. Scale bar, 100 μm. The lower panel is the percentage of TUNEL-positive cells. (**D**) WB using anticleaved caspase-3 and anti-ACTB. BEAS-2B *(Figure legend continues)*

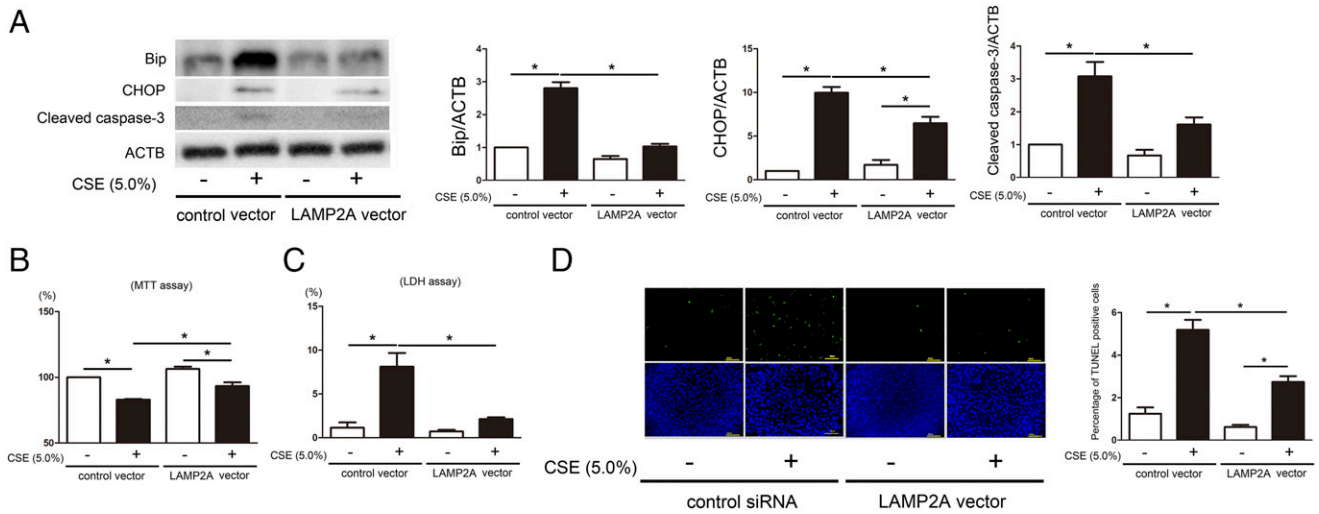


**FIGURE 5.** LAMP2A overexpression suppresses CSE-induced UPR and apoptosis. (**A**) Western blotting (WB) using anti-Bip, anti-CHOP, anticleaved caspase-3, and anti-ACTB. BEAS-2B cells were transfected with control or LAMP2A vector, and CSE treatment was started 48 h posttransfection. Cell lysates were collected after treatment with CSE (5%) for 24 h. The right panels show the average (±SEM) of relative expression, taken from densitometric analysis of WB ($n = 3$). (**B**) Viable cell count was evaluated by MTT assay. BEAS-2B cells were transfected with control or LAMP2A vector, and CSE (5%) treatment was started 48 h posttransfection. Viable cell count was assessed after 24-h treatment. (**C**) Cell cytotoxicity analysis of the LDH assay. Cytotoxicity was calculated by measuring the amount of LDH in the supernatant released from vector-transfected BEAS-2B cells after 24-h CSE (5%) treatment. (**D**) Photographs of fluorescence staining of the TUNEL assay of the control or LAMP2A vector transfected BEAS-2B cells after 24-h treatment with CSE (5%). DAPI (blue) and TUNEL-positive cells (green) are shown. Scale bar, 100 μm. The right panel is the percentage of TUNEL-positive cells. *$p < 0.05$ by ANOVA and Bonferroni posttest.

activation (Fig. 4A, 4B). Participation of CHOP in CSE-induced apoptosis, especially in the setting of reduced CMA, was examined by simultaneous CHOP and LAMP2A knockdown. LAMP2A siRNA was initially transfected and CHOP siRNA was subsequently transfected 24 h later in BEAS-2B cells. After an additional 24-h incubation, efficient knockdown of both LAMP2A and CHOP were confirmed by Western blotting (data not shown), and CSE treatment was performed for 24 h. Consistent with control BEAS-2B cells, CHOP knockdown significantly suppressed CSE-induced apoptosis in BEAS-2B cells with reduced CMA activity in the LAMP2A knockdown (Fig. 4C, 4D). In line with LAMP2A knockdown, Nrf2 knockdown clearly enhanced both CHOP and cleaved caspase-3 expression, further supporting the notion that the Nrf2–LAMP2A axis is responsible for regulating CHOP-mediated apoptosis during CSE exposure (Supplemental Fig. 3A).

To further clarify the role of CMA in CSE-induced apoptosis, LAMP2A overexpression experiments were performed. Transfection of LAMP2A expression vector efficiently overexpressed LAMP2A, and the subsequent enhanced CMA activity was demonstrated by a reduction of GAPDH protein levels (Supplemental Fig. 3B). LAMP2A overexpression clearly suppressed not only Bip and CHOP expression but also reduced levels of cleaved capase-3 during CSE exposure (Fig. 5A). LAMP2A overexpression significantly increased viable cell counts and reduced cell death (Fig. 5B–D), further supporting the notion that CMA induction of LAMP2A has a protective role in UPR caused by CSE exposure.

*Inspection of Nrf2–LAMP2A axis in COPD lungs*

To elucidate the clinical implication of impaired CMA and UPR in COPD pathogenesis, an immunohistochemical evaluation was conducted. In line with previous findings, Nrf2 expression levels were significantly reduced in SAEC in COPD lungs (Fig. 6A). Consistent with reduced Nrf2, LAMP2A expression levels were also significantly reduced in SAEC in COPD lungs (Fig. 6B). Because LAMP2A is a lysosomal protein and may reflect total lysosome numbers, levels of another type of lysosome-associated membrane protein, LAMP1, were examined. In contrast to LAMP2A, LAMP1 expression levels were significantly increased in SAEC (Fig. 6C), suggesting an accumulation of lysosomes with impaired CMA activity in COPD lungs. Although increased Bip was clearly demonstrated in SAEC in COPD lungs (Fig. 6D), CHOP expression was not detected in COPD lungs by means of immunohistochemical evaluation, which can be attributed to our technical limitation (data not shown). We also evaluated Nrf2 and LAMP2A expression levels in large airway epithelial cells. In line with SAEC, Nrf2 and LAMP2A expression levels were significantly reduced in the large airway epithelial cells of COPD lungs (Supplemental Fig. 4).

Nrf2 and LAMP2A expression levels were also evaluated in HBEC isolated from the bronchi of patients. Patient characteristics are presented in Table I. Consistent with immunohistochemical evaluation in SAEC, both Nrf2 and LAMP2A expression levels were significantly reduced in HBEC isolated from COPD lungs (Fig. 7A). Positive correlation between Nrf2 and LAMP2A expression levels was detected by linear regression analysis (Fig. 7B). Reduced Nrf2 and LAMP2A expression levels in HBEC from COPD lungs were further confirmed at mRNA levels (Fig. 7C, 7D). Next, we examined the correlation between LAMP2A expression levels in HBEC and clinical characteristics. Although no correlation with smoking index (SI) was detected, LAMP2A showed significant positive correlations with pulmonary function tests of the percentage of predicted forced

cells were transfected with control or LAMP2A and or CHOP siRNA. CSE (5%) treatment was started 24 h post-siRNA transfection. Cell lysates were collected after treatment with CSE (5%) for 24 h. The lower panel shows the average (±SEM) of relative expression, taken from densitometric analysis of WB ($n = 4$). *$p < 0.05$ by ANOVA and Bonferroni posttest.

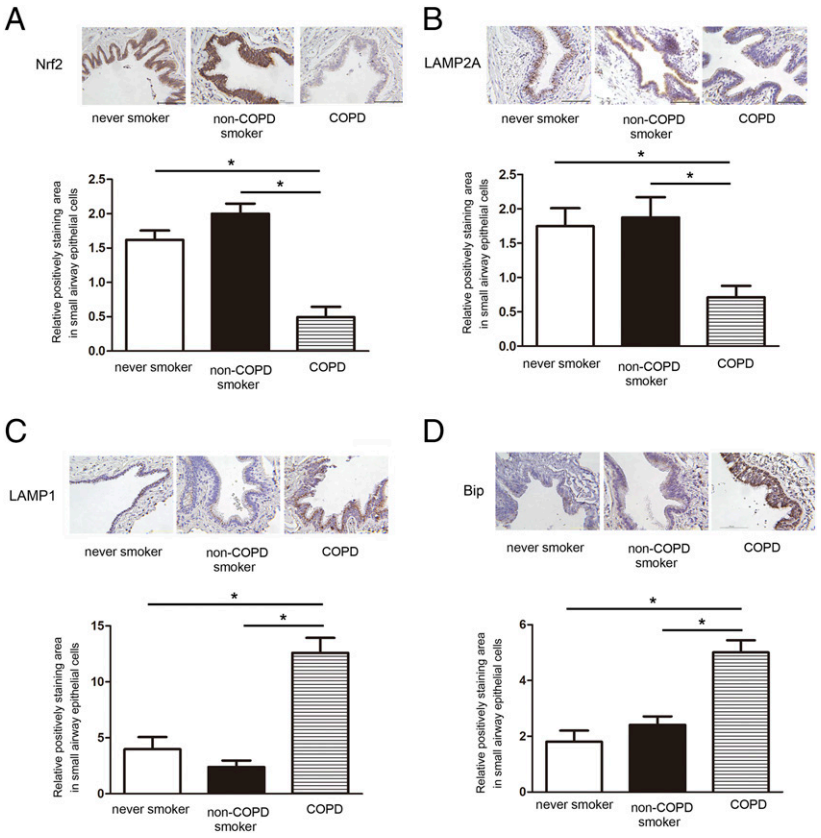


**FIGURE 6.** Reduced Nrf2 and LAMP2A and increased LAMP1 and Bip in COPD lungs. (**A**) Immunohistochemical staining of Nrf2 in nonsmoker, non-COPD smoker, and COPD lungs. Shown panels are low magnification view of original magnification ×100. Scale bar, 100 μm. The lower panel is the percentage of positively stained cells in small airways. (**B**) Immunohistochemical staining of LAMP2A in nonsmoker, non-COPD smoker, and COPD lungs. Scale bar, 100 μm. The lower panel is the percentage of positively stained cells in small airways. (**C**) Immunohistochemical staining of LAMP1 in nonsmoker, non-COPD smoker, and COPD lungs. Scale bar, 100 μm. The lower panel is the percentage of positively stained cells in small airways. (**D**) Immunohistochemical staining of Bip in nonsmoker, non-COPD smoker, and COPD lungs. Scale bar, 100 μm. The lower panel is the percentage of positively stained cells in small airways. *$p < 0.05$ by ANOVA and Bonferroni posttest.

expiratory volume in 1 s (%FEV1.0), indicating that LAMP2A is not simply associated with smoking status but is more directly linked to airway obstruction in COPD pathogenesis (Fig. 7E).

## Discussion

In the current study, we demonstrate the potential involvement of CMA in regulating UPR-mediated apoptosis as a part of COPD pathogenesis. CSE induces LAMP2A expression with concomitant CMA, and Nrf2 is responsible for regulating LAMP2A mRNA expression. Reduced CMA via LAMP2A knockdown enhances UPR and is accompanied by increased apoptosis, whereas CSE-induced UPR and apoptosis are clearly reversed by LAMP2A overexpression, suggesting the existence of functional cross-talk between UPR and CMA during CSE exposure. During UPR, participation of CHOP in CS-induced apoptosis in the setting of reduced CMA was confirmed by CHOP knockdown experiments. Compared with never smoker and non-COPD smoker, reduced Nrf2 and LAMP2A expression levels are demonstrated in SAEC in COPD lungs. In line with lung tissue evaluation, both Nrf2 and LAMP2A expression levels are significantly reduced in HBEC isolated from COPD patients, and their expression levels are positively correlated. LAMP2A expression levels in HBEC are significantly correlated with pulmonary function tests but not with SI. Taken together, impaired CMA modulated by Nrf2 may be causally associated with COPD development through enhanced UPR-mediated apoptosis in lung epithelial cells.

It has been reported that forced Nrf2 expression prevents CMA decline and showed a neuroprotective effect in a mouse model of Parkinson disease (27). A recent paper demonstrated that Nrf2 upregulates LAMP2A expression levels through binding to *LAMP2A* gene (15). In line with those papers, knockdown experiments showed that Nrf2 is at least partly responsible for upregulating LAMP2A expression at mRNA levels during CSE exposure in in vitro HBEC models (Fig. 1). We also observed significant reduction in both Nrf2 and LAMP2A protein levels in SAEC in COPD lungs and in HBEC derived from COPD patients (Figs. 6, 7), further supporting the notion of the upstream regulatory role for Nrf2 in LAMP2A expression in COPD pathogenesis. Intriguingly, decreased LAMP2A expression levels have been demonstrated in brain tissue from Parkinson disease patients, which can be attributed to both a sequence variant in the LAMP2A promoter region and an increase in a specific microRNA (miRNA) targeting LAMP2A (28, 29). Although reported miRNAs for LAMP2A regulation have not been implicated in COPD pathogenesis (29, 30), it is plausible that alterations in the promoter region and targeting via miRNA are involved in the mechanisms

Table I. Patient characteristics (for HBEC)

| | Nonsmoker ($n$ = 8) | Non-COPD Smoker ($n$ = 7) | COPD ($n$ = 9) | $p$ Value |
|---|---|---|---|---|
| Age, y | 72.6 ± 4.7 | 65.0 ± 8.4 | 67.0 ± 9.6 | NS |
| Male, % of group | 12.5 | 85.7 | 100.0 | <0.0001* |
| SI (pack-y) | 0 | 19.7 ± 14.0 | 56.7 ± 33.4 | <0.0001** |
| FEV1.0/FVC (%) | 77.3 ± 4.4 | 83.5 ± 12.8 | 63.2 ± 5.0 | <0.0001** |
| %FEV1.0 | 105.6 ± 18.4 | 94.5 ± 16.1 | 89.7 ± 9.5 | 0.104** |

FEV1.0, forced expiratory volume in 1 s; FVC, forced vital capacity; NS, not statistically significant.
Values are mean ± SD. *$\chi^2$ test for independence, **ANOVA and Bonferroni posttest.

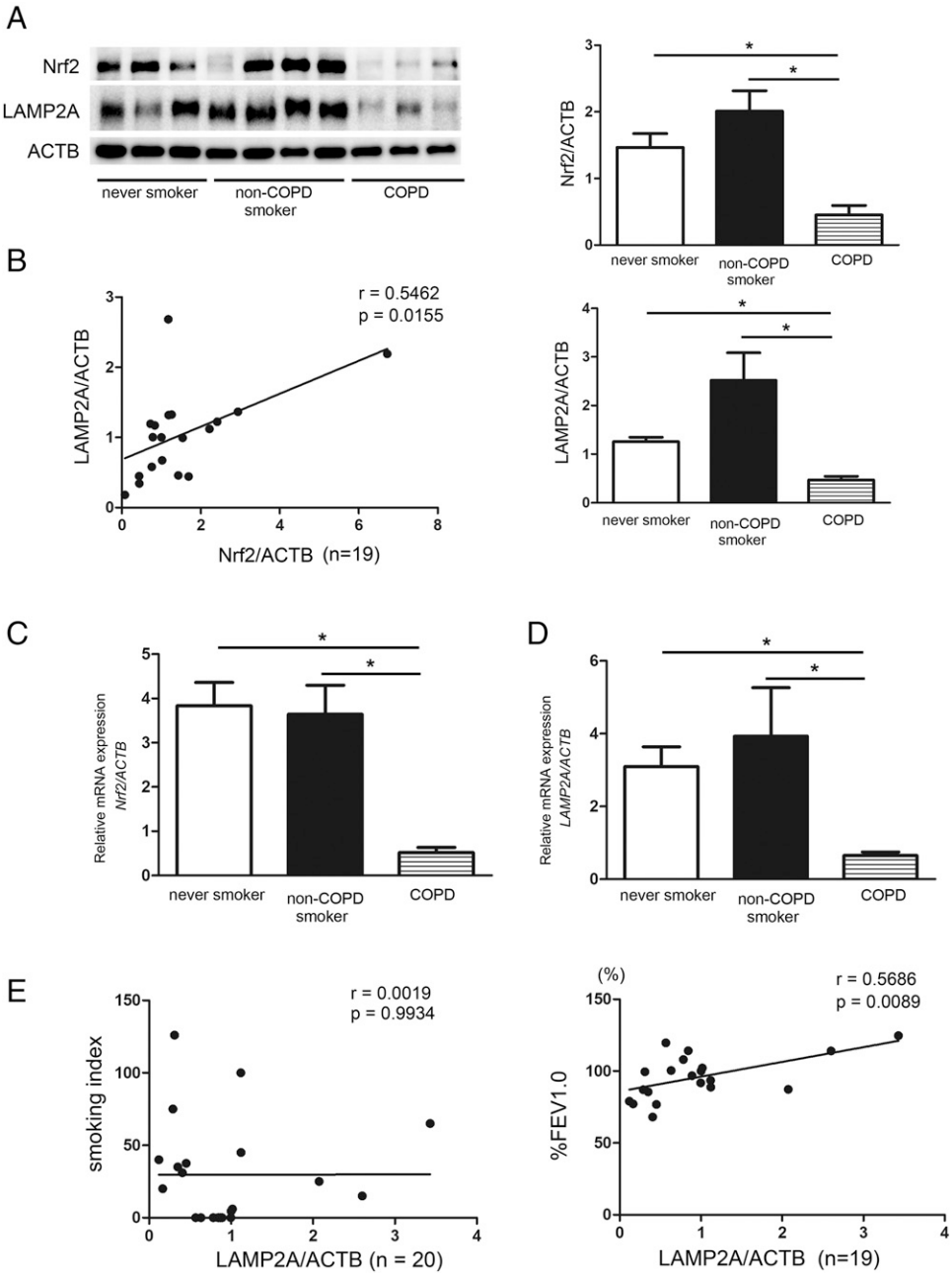


**FIGURE 7.** Reduced Nrf2 and LAMP2A in COPD HBEC. (**A**) Western blotting (WB) using anti-Nrf2, anti-LAMP2A, and anti-ACTB of HBEC lysates. The right panels show the average (±SEM) of relative expression, taken from densitometric analysis of WB (nonsmoker = 7, non-COPD smoker = 8, and COPD = 7). (**B**) Shown is the relationship between Nrf2 and LAMP2A normalized to ACTB. HBEC are from nonsmoker ($n$ = 6), non-COPD smoker ($n$ = 7), and COPD ($n$ = 6) patients. Linear regression analysis was used to compare Nrf2 expression levels to LAMP2A expression levels in HBEC. (**C**) Real-time PCR using primers to Nrf2 or ACTB as a control. RNA samples were collected from HBEC (nonsmoker = 6, non-COPD smoker = 4, and COPD = 6). Nrf2 mRNA expression was normalized to ACTB. Shown is the fold increase (±SEM) relative to control-treated cells ($n$ = 3). (**D**) Real-time PCR using primers to LAMP2A or ACTB as a control. RNA samples were collected from HBEC (nonsmoker = 6, non-COPD smoker = 4, and COPD = 6). LAMP2A mRNA expression was normalized to ACTB. Shown is the fold increase (±SEM) relative to control-treated cells ($n$ = 3). (**E**) Shown is the relationship between relative LAMP2A expression normalized to ACTB in HBEC and SI and %FEV1.0, respectively. HBEC are from nonsmoker, non-COPD smoker, and COPD patients. Linear regression analysis was used to compare LAMP2A expression levels in HBEC to SI and pulmonary function test. *$p < 0.05$ by ANOVA and Bonferroni posttest.

for LAMP2A reduction in COPD lungs. Furthermore, an age-dependent decline in CMA activity conferred by reduced LAMP2A expression levels was demonstrated in a variety of human cell types, with the thought that lower stability at the lysosomal membrane caused by alterations in lipid composition is responsible for this decline (16, 31, 32). COPD is a representative pulmonary disorder associated with aging, hence reduced LAMP2A in COPD lungs can be regulated not only at the mRNA level but also by a variety of posttranscriptional modifications associated with aging.

Target selectivity of CMA has been implicated in the timed degradation of specific proteins involved in the regulation of enzymatic metabolic processes and subsets of transcriptional programs (33). Additionally, the activation of CMA has also been demonstrated to remove malfunctional and unfolded proteins during oxidative stress, indicating that CMA may have a regulatory

role in multiple cellular processes not only for maintaining nutritional homeostasis but also for adapting the cell to stressed conditions (32, 34, 35). UPR is activated by inappropriate protein folding in the lumen of the ER caused by cellular stressors, including oxidative stress (3). UPR promotes adaptive mechanisms for cell survival but also induces apoptosis in the setting of excessive ER stress (5). The ER and lysosome are the most critical organelles, which are responsible for sensing and regulating cellular stress responses (36); hence, functional cross-talk between the ER and lysosomes is likely to exist, especially in the setting of excessive oxidative stress. Intriguingly, a recent paper demonstrated a functional link between ER stress and CMA, which showed that increased ER stress is a part of the mechanism of CMA activation via an increase in LAMP2A phosphorylation (22). In line with previous findings, CS induced both UPR and CMA activation of LAMP2A upregulation in our experimental conditions (Figs. 1, 3) (3, 4, 23). Importantly, we clearly showed the novel functional cross-talk between UPR and CMA during CSE exposure in this study (Figs. 3, 4). Impaired CMA due to LAMP2A knockdown resulted in enhanced UPR, including CHOP expression accompanied by increased apoptosis. Also, LAMP2A overexpression leading to CMA activation reduced both UPR and apoptosis in response to CSE exposure. Although the precise mechanism for UPR regulation by CMA remains unclear, we speculate the following possibilities. First, CMA-mediated elimination of damaged proteins has a preventive and regulatory role for CSE-induced ER stress. Second, like ER-associated degradation by proteasomes, CMA may have a specific role in the removal of unfolded proteins from the stressed ER. Third, CMA activation is responsible for selective degradation of the UPR components responsible for attenuating UPR-mediated cytotoxic response during CSE exposure. Although these possibilities should be explored in future studies, it remains likely that CMA regulation of UPR has a critical role in maintaining cellular survival during the oxidative stress of CS exposure.

CSE led to the accumulation of lysosomes in lung epithelial cells, which may represent phenotypic alteration to cellular senescence (37). We have reported accelerated cellular senescence in SAEC in COPD lungs, and immunohistochemistry demonstrated increased expression levels of LAMP1 (Fig. 5) (38, 39). LAMP1 is a major lysosomal membrane protein and is considered to be representative of the total number of lysosomes. Accordingly, it is plausible that an increase in LAMP1 may reflect the accumulation of lysosomes in SAEC with accelerated cellular senescence in COPD lungs. In contrast to LAMP1, LAMP2A expression levels were clearly reduced in SAEC in COPD lungs (Fig. 5). LAMP2A expression is not considered to correlate with total lysosome numbers, and it is likely that increased LAMP1 accompanied by LAMP2A reduction may reflect the accumulation of CMA-inactive lysosomes in SAEC in COPD lungs. It has been reported that lysosomal function declines with aging, and lysosomal dysfunction is causally linked to the pathogenesis of age-related disorders including neurodegenerative diseases (40, 41). Therefore, we speculate that the accumulation of CMA-inactive dysfunctional lysosomes can be a representative feature of accelerated cellular senescence pathologically linked with aging-associated disorders, including COPD. Autophagic response to eliminate damaged lysosomes, known as lysophagy, plays an essential role in maintaining lysosomal functional integrity; hence, the causal link between lysophagy status and accumulation of CMA-inactive lysosomes is a potentially interesting topic of research for further understanding the functional interplay between macropautophagy and CMA during aging (42, 43).

In conclusion, our findings indicate the participation of reduced CMA-mediated lung epithelial cell apoptosis in COPD pathogenesis. To our knowledge, this study is the first report showing the existence of functional cross-talk between CMA and UPR in terms of regulating apoptosis during CS exposure. It is likely that activating CMA can be a promising target for developing an antiapoptotic modality of COPD treatment.

## Acknowledgments

We thank Stephanie Cambier (University of Washington, Seattle, WA) for technical support.

## Disclosures

The authors have no financial conflicts of interest.

## References

1. Barnes, P. J. 2017. Senescence in COPD and its comorbidities. *Annu. Rev. Physiol.* 79: 517–539.
2. Yamada, K., K. Asai, F. Nagayasu, K. Sato, N. Ijiri, N. Yoshii, Y. Imahashi, T. Watanabe, Y. Tochino, H. Kanazawa, and K. Hirata. 2016. Impaired nuclear factor erythroid 2-related factor 2 expression increases apoptosis of airway epithelial cells in patients with chronic obstructive pulmonary disease due to cigarette smoking. *BMC Pulm. Med.* 16: 27.
3. Kelsen, S. G., X. Duan, R. Ji, O. Perez, C. Liu, and S. Merali. 2008. Cigarette smoke induces an unfolded protein response in the human lung: a proteomic approach. *Am. J. Respir. Cell Mol. Biol.* 38: 541–550.
4. Jorgensen, E., A. Stinson, L. Shan, J. Yang, D. Gietl, and A. P. Albino. 2008. Cigarette smoke induces endoplasmic reticulum stress and the unfolded protein response in normal and malignant human lung cells. *BMC Cancer* 8: 229.
5. Kelsen, S. G. 2016. The unfolded protein response in chronic obstructive pulmonary disease. *Ann. Am. Thorac. Soc.* 13(Suppl. 2): S138–S145.
6. Yokohori, N., K. Aoshiba, and A. Nagai; Respiratory Failure Research Group in Japan. 2004. Increased levels of cell death and proliferation in alveolar wall cells in patients with pulmonary emphysema. *Chest* 125: 626–632.
7. Min, T., M. Bodas, S. Mazur, and N. Vij. 2011. Critical role of proteostasis-imbalance in pathogenesis of COPD and severe emphysema. *J. Mol. Med. (Berl.)* 89: 577–593.
8. Tsai, M. J., W. A. Chang, S. F. Jian, K. F. Chang, C. C. Sheu, and P. L. Kuo. 2018. Possible mechanisms mediating apoptosis of bronchial epithelial cells in chronic obstructive pulmonary disease - a next-generation sequencing approach. *Pathol. Res. Pract.* 214: 1489–1496.
9. Gogebakan, B., R. Bayraktar, M. Ulaslı, S. Oztuzcu, D. Tasdemir, and H. Bayram. 2014. The role of bronchial epithelial cell apoptosis in the pathogenesis of COPD. *Mol. Biol. Rep.* 41: 5321–5327.
10. Hodge, S., G. Hodge, M. Holmes, and P. N. Reynolds. 2005. Increased airway epithelial and T-cell apoptosis in COPD remains despite smoking cessation. *Eur. Respir. J.* 25: 447–454.
11. Cullinan, S. B., and J. A. Diehl. 2004. PERK-dependent activation of Nrf2 contributes to redox homeostasis and cell survival following endoplasmic reticulum stress. *J. Biol. Chem.* 279: 20108–20117.
12. Zhao, H., S. Eguchi, A. Alam, and D. Ma. 2017. The role of nuclear factor-erythroid 2 related factor 2 (Nrf-2) in the protection against lung injury. *Am. J. Physiol. Lung Cell. Mol. Physiol.* 312: L155–L162.
13. Suzuki, M., T. Betsuyaku, Y. Ito, K. Nagai, Y. Nasuhara, K. Kaga, S. Kondo, and M. Nishimura. 2008. Down-regulated NF-E2-related factor 2 in pulmonary macrophages of aged smokers and patients with chronic obstructive pulmonary disease. *Am. J. Respir. Cell Mol. Biol.* 39: 673–682.
14. Rangasamy, T., C. Y. Cho, R. K. Thimmulappa, L. Zhen, S. S. Srisuma, T. W. Kensler, M. Yamamoto, I. Petrache, R. M. Tuder, and S. Biswal. 2004. Genetic ablation of Nrf2 enhances susceptibility to cigarette smoke-induced emphysema in mice. *J. Clin. Invest.* 114: 1248–1259.
15. Pajares, M., A. I. Rojo, E. Arias, A. Díaz-Carretero, A. M. Cuervo, and A. Cuadrado. 2018. Transcription factor NFE2L2/NRF2 modulates chaperone-mediated autophagy through the regulation of LAMP2A. *Autophagy* 14: 1310–1322.
16. Kaushik, S., and A. M. Cuervo. 2018. The coming of age of chaperone-mediated autophagy. *Nat. Rev. Mol. Cell Biol.* 19: 365–381.
17. Chen, Z. H., H. P. Kim, F. C. Sciurba, S. J. Lee, C. Feghali-Bostwick, D. B. Stolz, R. Dhir, R. J. Landreneau, M. J. Schuchert, S. A. Yousem, et al. 2008. Egr-1 regulates autophagy in cigarette smoke-induced chronic obstructive pulmonary disease. *PLoS One* 3: e3316.
18. Fujii, S., H. Hara, J. Araya, N. Takasaka, J. Kojima, S. Ito, S. Minagawa, Y. Yumino, T. Ishikawa, T. Numata, et al. 2012. Insufficient autophagy promotes bronchial epithelial cell senescence in chronic obstructive pulmonary disease. *OncoImmunology* 1: 630–641.
19. Mizumura, K., S. M. Cloonan, K. Nakahira, A. R. Bhashyam, M. Cervo, T. Kitada, K. Glass, C. A. Owen, A. Mahmood, G. R. Washko, et al. 2014. Mitophagy-dependent necroptosis contributes to the pathogenesis of COPD. *J. Clin. Invest.* 124: 3987–4003.
20. Araya, J., K. Tsubouchi, N. Sato, S. Ito, S. Minagawa, H. Hara, Y. Hosaka, A. Ichikawa, N. Saito, T. Kadota, et al. 2019. PRKN-regulated mitophagy and cellular senescence during COPD pathogenesis. *Autophagy* 15: 510–526.

21. Kaushik, S., A. C. Massey, N. Mizushima, and A. M. Cuervo. 2008. Constitutive activation of chaperone-mediated autophagy in cells with impaired macroautophagy. *Mol. Biol. Cell* 19: 2179–2192.
22. Li, W., J. Zhu, J. Dou, H. She, K. Tao, H. Xu, Q. Yang, and Z. Mao. 2017. Phosphorylation of LAMP2A by p38 MAPK couples ER stress to chaperone-mediated autophagy. *Nat. Commun.* 8: 1763.
23. Lee, C. H., K. H. Lee, A. H. Jang, and C. G. Yoo. 2017. The impact of autophagy on the cigarette smoke extract-induced apoptosis of bronchial epithelial cells. *Tuberc. Respir. Dis. (Seoul)* 80: 83–89.
24. Araya, J., S. Cambier, J. A. Markovics, P. Wolters, D. Jablons, A. Hill, W. Finkbeiner, K. Jones, V. C. Broaddus, D. Sheppard, et al. 2007. Squamous metaplasia amplifies pathologic epithelial-mesenchymal interactions in COPD patients. *J. Clin. Invest.* 117: 3551–3562.
25. Tsubouchi, K., J. Araya, S. Minagawa, H. Hara, A. Ichikawa, N. Saito, T. Kadota, N. Sato, M. Yoshida, Y. Kurita, et al. 2017. Azithromycin attenuates myofibroblast differentiation and lung fibrosis development through proteasomal degradation of NOX4. *Autophagy* 13: 1420–1434.
26. Pajares, M., N. Jiménez-Moreno, A. J. García-Yagüe, M. Escoll, M. L. de Ceballos, F. Van Leuven, A. Rábano, M. Yamamoto, A. I. Rojo, and A. Cuadrado. 2016. Transcription factor NFE2L2/NRF2 is a regulator of macroautophagy genes. *Autophagy* 12: 1902–1916.
27. Gan, L., M. R. Vargas, D. A. Johnson, and J. A. Johnson. 2012. Astrocyte-specific overexpression of Nrf2 delays motor pathology and synuclein aggregation throughout the CNS in the alpha-synuclein mutant (A53T) mouse model. *J. Neurosci.* 32: 17775–17787.
28. Pang, S., D. Chen, A. Zhang, X. Qin, and B. Yan. 2012. Genetic analysis of the LAMP-2 gene promoter in patients with sporadic Parkinson's disease. *Neurosci. Lett.* 526: 63–67.
29. Alvarez-Erviti, L., Y. Seow, A. H. V. Schapira, M. C. Rodriguez-Oroz, J. A. Obeso, and J. M. Cooper. 2013. Influence of microRNA deregulation on chaperone-mediated autophagy and α-synuclein pathology in Parkinson's disease. *Cell Death Dis.* 4: e545.
30. Alipoor, S. D., I. M. Adcock, J. Garssen, E. Mortaz, M. Varahram, M. Mirsaeidi, and A. Velayati. 2016. The roles of miRNAs as potential biomarkers in lung diseases. *Eur. J. Pharmacol.* 791: 395–404.
31. Cuervo, A. M., and J. F. Dice. 2000. Age-related decline in chaperone-mediated autophagy. *J. Biol. Chem.* 275: 31505–31513.
32. Cuervo, A. M., and E. Wong. 2014. Chaperone-mediated autophagy: roles in disease and aging. *Cell Res.* 24: 92–104.
33. Cuervo, A. M., L. Stefanis, R. Fredenburg, P. T. Lansbury, and D. Sulzer. 2004. Impaired degradation of mutant alpha-synuclein by chaperone-mediated autophagy. *Science* 305: 1292–1295.
34. Kiffin, R., C. Christian, E. Knecht, and A. M. Cuervo. 2004. Activation of chaperone-mediated autophagy during oxidative stress. *Mol. Biol. Cell* 15: 4829–4840.
35. Massey, A. C., S. Kaushik, G. Sovak, R. Kiffin, and A. M. Cuervo. 2006. Consequences of the selective blockage of chaperone-mediated autophagy. *Proc. Natl. Acad. Sci. USA* 103: 5805–5810.
36. Li, W., Q. Yang, and Z. Mao. 2018. Signaling and induction of chaperone-mediated autophagy by the endoplasmic reticulum under stress conditions. *Autophagy* 14: 1094–1096.
37. Tsuji, T., K. Aoshiba, and A. Nagai. 2006. Alveolar cell senescence in patients with pulmonary emphysema. *Am. J. Respir. Crit. Care Med.* 174: 886–893.
38. Ito, S., J. Araya, Y. Kurita, K. Kobayashi, N. Takasaka, M. Yoshida, H. Hara, S. Minagawa, H. Wakui, S. Fujii, et al. 2015. PARK2-mediated mitophagy is involved in regulation of HBEC senescence in COPD pathogenesis. *Autophagy* 11: 547–559.
39. Saito, N., J. Araya, S. Ito, K. Tsubouchi, S. Minagawa, H. Hara, A. Ito, T. Nakano, Y. Hosaka, A. Ichikawa, et al. 2019. Involvement of lamin B1 reduction in accelerated cellular senescence during chronic obstructive pulmonary disease pathogenesis. *J. Immunol.* 202: 1428–1440.
40. Carmona-Gutierrez, D., A. L. Hughes, F. Madeo, and C. Ruckenstuhl. 2016. The crucial impact of lysosomes in aging and longevity. *Ageing Res. Rev.* 32: 2–12.
41. Lawrence, R. E., and R. Zoncu. 2019. The lysosome as a cellular centre for signalling, metabolism and quality control. *Nat. Cell Biol.* 21: 133–142.
42. Hung, Y. H., L. M. Chen, J. Y. Yang, and W. Y. Yang. 2013. Spatiotemporally controlled induction of autophagy-mediated lysosome turnover. *Nat. Commun.* 4: 2111.
43. Maejima, I., A. Takahashi, H. Omori, T. Kimura, Y. Takabatake, T. Saitoh, A. Yamamoto, M. Hamasaki, T. Noda, Y. Isaka, and T. Yoshimori. 2013. Autophagy sequesters damaged lysosomes to control lysosomal biogenesis and kidney injury. *EMBO J.* 32: 2336–2347.

Supplementary Figure 1.

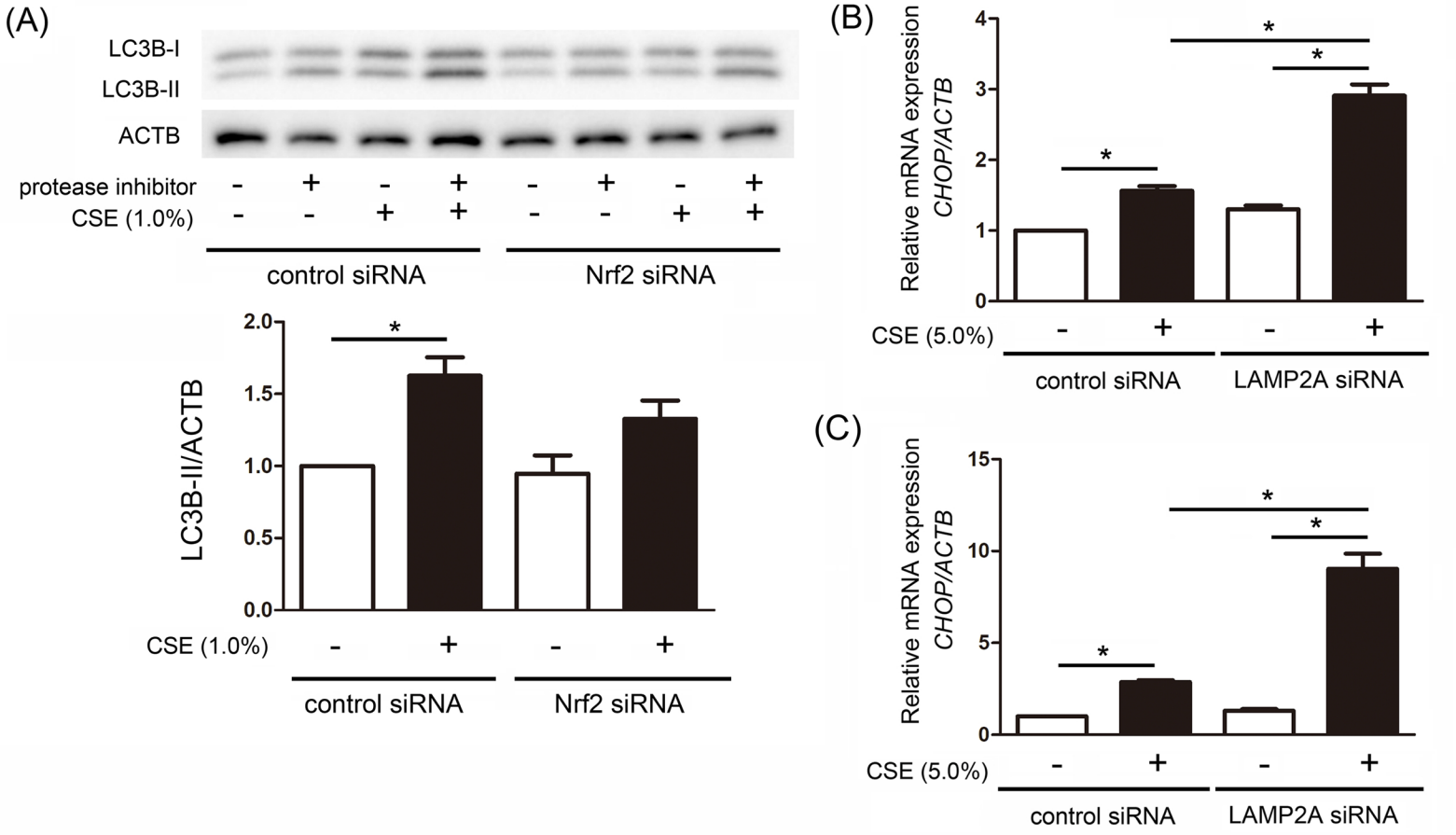


**Supplementray Figure 1. Effect of Nrf2 and LAMP2A knockdown**

**Effect of Nrf2 knockdown on CSE-induced macroautophagy.**

(A) WB using anti-LC3B and ACTB. HBEC were transfected with control siRNA or Nrf2 siRNA. CSE (1%) treatment was started 24 h post-transfection and protein samples were collected after 24 h treatment. Protease inhibitor (E64d 10 μg/ml, pepstatin A 10 μg/ml) treatment was started 6h before collecting cell lysates.Shown is a representative experiment of 3 showing similar results. The lower panel is the average (±SEM) relative increase in LC3B-II normalized to ACTB in the presence of protease inhibitor, which are taken from densitometric analysis of WB from three independent experiments. *p<0.05, by by ANOVA and Bonferroni's post-test.

**Effect of LAMP2A Knockdown on CHOP mRNA expression.**

(B) BEAS-2B cells were transfected with control siRNA or LAMP2A siRNA and CSE treatment was started 48 h psot siRNA transfection. RNA samples were collected after treatment with CSE (5%) for 24 h. Realtime-PCR was performed using primers to CHOP.or ACTB as a control. CHOP mRNA expression was normalized to ACTB. Shown is the fold increase(±SEM) retaive to control treated cells (n=3). *p<0.05, by by ANOVA and Bonferroni's post-test. (C) HBEC were transfected with control siRNA or LAMP2A siRNA and CSE treatment was started 48 h psot siRNA transfection. RNA samples were collected after treatment with CSE (5%) for 24 h. Realtime-PCR was performed using primers to CHOP.or ACTB as a control. CHOP mRNA expression was normalized to ACTB. Shown is the fold increase(±SEM) retaive to control treated cells (n=3). *p<0.05, by by ANOVA and Bonferroni's post-test.

Supplementary Figure 2.

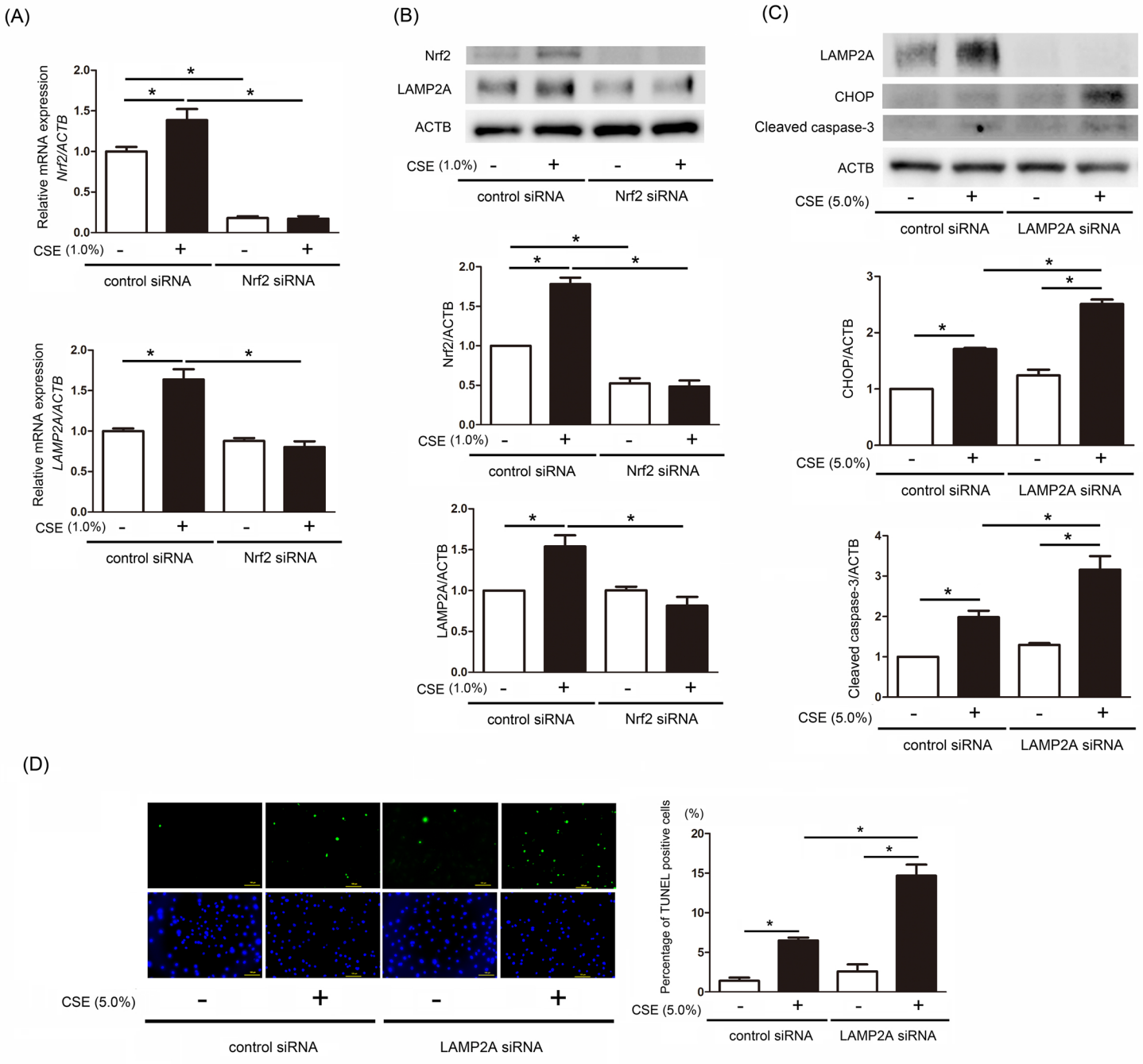


**Supplementary Figure 2. Effect of Nrf2 and LAMP2A knockdown in small airway epithelial cells (SAEC).** (A)Real time-PCR was performed using primers to Nrf2, LAMP2A, or ACTB as a control. SAEC were transfected with control or Nrf2 siRNA and CSE treatment was started 48 h post siRNA transfection. RNA samples were collected after treatment with CSE (1%) for 24 h. Nrf2 mRNA expression was normalized to ACTB. Shown is the fold increase (±SEM) relative to control treated cells (n=3). *P < 0.05, by ANOVA and Bonferroni's post-test. (B) WB using anti-Nrf2, anti-LAMP2A, and anti-ACTB . SAEC were transfected with control or Nrf2 siRNA and CSE treatment was started 48 h post siRNA transfection. Cell lysates were collected after treatment with CSE (1%) for 48 h. The lower panels shows the average (±SEM) of relative expression, taken from densitometric analysis of WB (n=3). *P < 0.05, by ANOVA and Bonferroni's post-test. (C) WB using anti-LAMP2A, anti-CHOP, anti-cleaved caspase-3, and anti-ACTB. SAEC were transfected with control or LAMP2A siRNA and CSE treatment was started 48 h post siRNA transfection. Cell lysates were collected after treatment with CSE (5%) for 24 h. The lower panels show the average (±SEM) of relative expression, taken from densitometric analysis of WB (n=3). *P < 0.05, by ANOVA and Bonferroni's post-test. (D) Photographs of fluorescence staining of the TUNEL assay of the control or LAMP2A siRNA transfected HBEC after 24 h treatment with CSE (5%). DAPI (blue) and TUNEL-positive cells (green) are shown. Scale bars, 100 μm. The right panel is the percentage of TUNEL-positive cells. *P < 0.05, by ANOVA and Bonferroni's post-test.

Supplementary Figure 3.

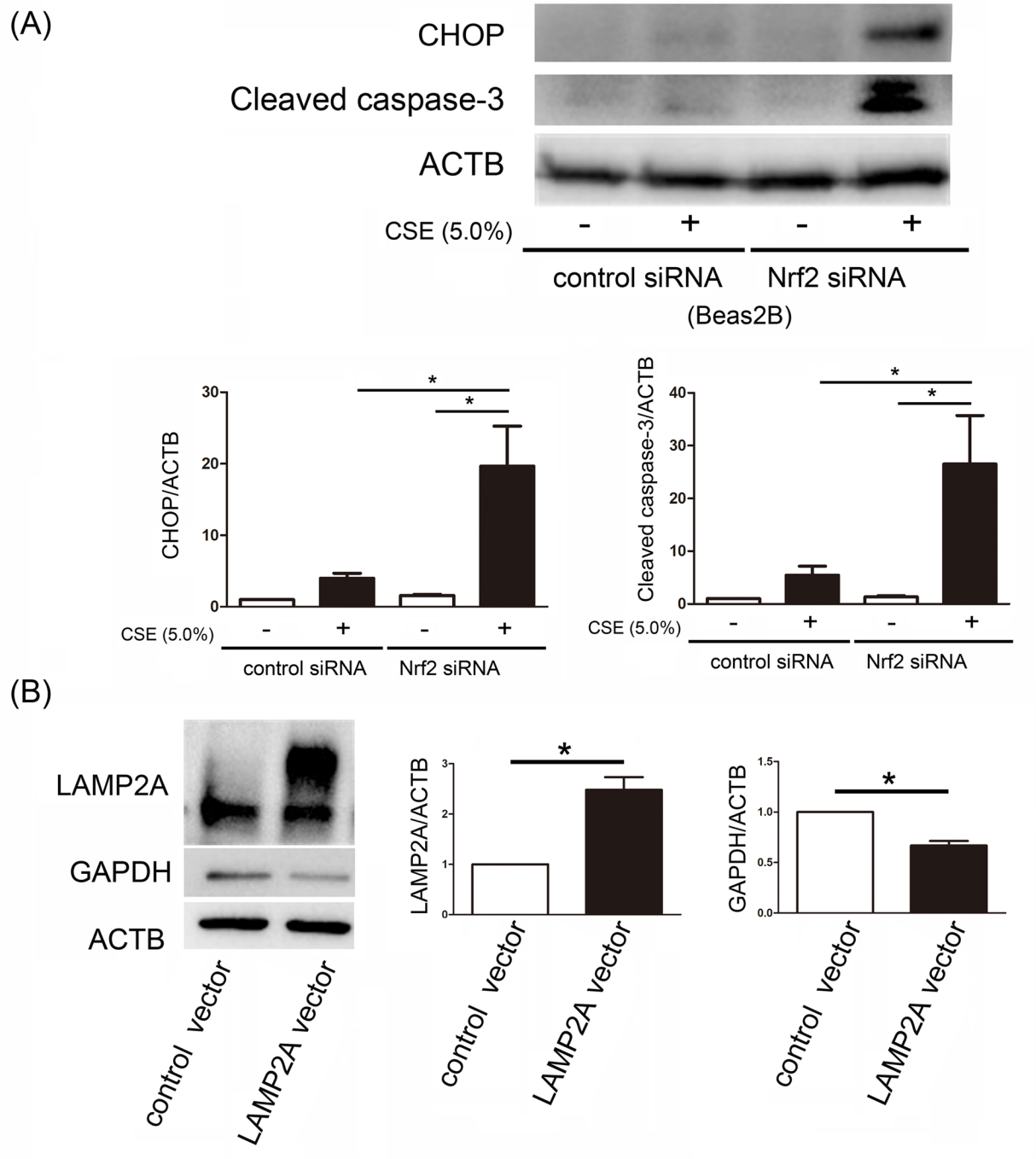


**Supplementary Figure 3. Effect of Nrf2 knockdown and LAMP2A overexpression.**

(A) **Effect of Nrf2 knockdown on CHOP and cleaved caspase-3 expression.** WB using anti-CHOP, anti-cleaved caspase-3, and anti-ACTB. BEAS-2B cells were transfected with control or Nrf2 siRNA. CSE treatment was started 48 h post siRNA transfection. Cell lysates were collected after treatment with CSE (5%) for 24 h. The lower panels show the average (±SEM) of relative expression, which are taken from densitometric analysis of WB (n=3). *p<0.05, by by ANOVA and Bonferroni's post-test.

(B) **Effect of LAMP2A overexpression on GAPDH expession.**

WB using anti-LAMP2A, anti-GAPDH, and anti-ACTB. BEAS-2B cells were transfected with control or LAMP2A vector and cell lysates were collected 48 h psot transfection.The right panels show the average (±SEM) of relative expression, which are taken from densitometric analysis of WB (n=3). *p<0.05, by by ANOVA and Bonferroni's post-test.

Supplementary Figure 4.

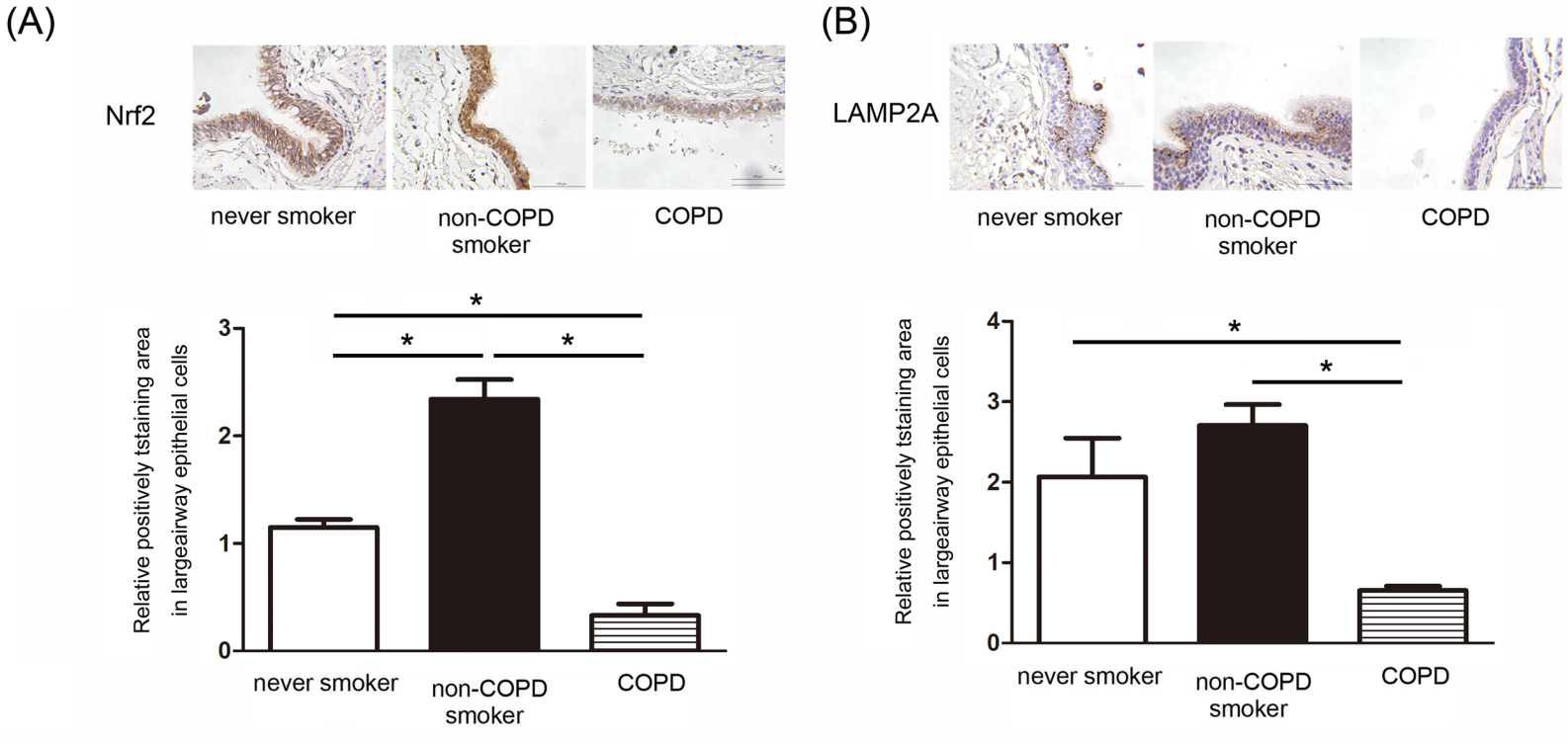


**Supplementary Figure 4. Reduced Nrf2 and LAMP2A in bronchial epithelial cells in COPD lungs.**

(A) Immunohistochemical staining of Nrf2 in non-smoker, non-COPD smoker, and COPD lungs. Shown panels are low magnification view of original magnification ×100. Bar = 100 μm. The lower panel is the percentage of positively stained cells in large airways. *P < 0.05, by ANOVA and Bonferroni's post-test. (B) Immunohistochemical staining of LAMP2A in non-smoker, non-COPD smoker, and COPD lungs. Bar = 100 μm. The lower panel is the percentage of positively stained cells in large airways. *P < 0.05, by ANOVA and Bonferroni's post-test.